University of Massachusetts Medical School
eScholarship@UMMS

Open Access Articles | Open Access Publications by UMMS Authors

6-27-2002

Spontaneous transient outward currents arise from microdomains where BK channels are exposed to a mean Ca(2+) concentration on the order of 10 microM during a Ca(2+) spark

Ronghua ZhuGe
University of Massachusetts Medical School

Kevin E. Fogarty
University of Massachusetts Medical School

Richard A. Tuft
University of Massachusetts Medical School

See next page for additional authors

Follow this and additional works at: http://escholarship.umassmed.edu/oapubs

 Part of the Engineering Physics Commons, and the Physiology Commons

Repository Citation

ZhuGe, Ronghua; Fogarty, Kevin E.; Tuft, Richard A.; and Walsh, John V., "Spontaneous transient outward currents arise from microdomains where BK channels are exposed to a mean Ca(2+) concentration on the order of 10 microM during a Ca(2+) spark" (2002). *Open Access Articles*. 1063.
http://escholarship.umassmed.edu/oapubs/1063

This material is brought to you by eScholarship@UMMS. It has been accepted for inclusion in Open Access Articles by an authorized administrator of eScholarship@UMMS. For more information, please contact Lisa.Palmer@umassmed.edu.

Spontaneous transient outward currents arise from microdomains where BK channels are exposed to a mean Ca(2+) concentration on the order of 10 microM during a Ca(2+) spark

Authors
Ronghua ZhuGe, Kevin E. Fogarty, Richard A. Tuft, and John V. Walsh

This article is available at eScholarship@UMMS: http://escholarship.umassmed.edu/oapubs/1063

Published June 10, 2002

Spontaneous Transient Outward Currents Arise from Microdomains Where BK Channels Are Exposed to a Mean Ca^{2+} Concentration on the Order of 10 μM during a Ca^{2+} Spark

Ronghua ZhuGe, Kevin E. Fogarty, Richard A. Tuft, and John V. Walsh, Jr

Biomedical Imaging Group, Department of Physiology, University of Massachusetts Medical School, Worcester, MA 01655

ABSTRACT Ca^{2+} sparks are small, localized cytosolic Ca^{2+} transients due to Ca^{2+} release from sarcoplasmic reticulum through ryanodine receptors. In smooth muscle, Ca^{2+} sparks activate large conductance Ca^{2+}-activated K^+ channels (BK channels) in the spark microdomain, thus generating spontaneous transient outward currents (STOCs). The purpose of the present study is to determine experimentally the level of Ca^{2+} to which the BK channels are exposed during a spark. Using tight seal, whole-cell recording, we have analyzed the voltage-dependence of the STOC conductance ($g_{(STOC)}$), and compared it to the voltage-dependence of BK channel activation in excised patches in the presence of different [Ca^{2+}]s. The Ca^{2+} sparks did not change in amplitude over the range of potentials of interest. In contrast, the magnitude of $g_{(STOC)}$ remained roughly constant from 20 to −40 mV and then declined steeply at more negative potentials. From this and the voltage dependence of BK channel activation, we conclude that the BK channels underlying STOCs are exposed to a mean [Ca^{2+}] on the order of 10 μM during a Ca^{2+} spark. The membrane area over which a concentration ≥10 μM is reached has an estimated radius of 150–300 nm, corresponding to an area which is a fraction of one square micron. Moreover, given the constraints imposed by the estimated channel density and the Ca^{2+} current during a spark, the BK channels do not appear to be uniformly distributed over the membrane but instead are found at higher density at the spark site.

KEY WORDS: calcium signaling • ion channel • STOC • sarcoplasmic reticulum • smooth muscle

Downloaded from www.jgp.org on July 15, 2008

INTRODUCTION

In smooth muscle and in neurons, Ca^{2+}-activated K^+ channels in the plasma membrane open in response to a highly localized cytosolic elevation in Ca^{2+} released from intracellular stores. In neurons the resulting K^+ current, designated as a spontaneous, miniature outward current, has been recorded (Brown et al., 1983), whereas the underlying Ca^{2+} transient has only been inferred but not observed directly. In smooth muscle cells, this K^+ current is designated as a spontaneous transient outward current (STOC)* (Benham and Bolton, 1986), and is due to the opening of large conductance Ca^{2+}-activated K^+ channels (BK channels). Moreover, in smooth muscle, not only have the STOCs been observed directly, but the underlying Ca^{2+} transients, which are designated as Ca^{2+} sparks, have been observed as well (Nelson et al., 1995; Mironneau et al., 1996; Bolton and Gordienko, 1998; ZhuGe et al., 1998a; Kirber et al., 2001). Ca^{2+} sparks result from focal Ca^{2+} release into the cytosol from the sarcoplasmic reticulum (SR) by the opening of a cluster of ryanodine receptors (RyRs).

The precise relationship between a Ca^{2+} spark and the STOC which it generates has attracted considerable attention for two reasons. First, STOCs provide a mechanism for vascular smooth muscle relaxation by driving the membrane potential more negative, thereby closing L-type Ca^{2+} channels which appear to supply the Ca^{2+} to initiate contraction. This mechanism of spark-induced relaxation, proposed originally for vascular smooth muscle by Nelson et al. (1995), has recently been confirmed in striking fashion using knock-out mice lacking the β1 subunit of the BK channels (Brenner et al., 2000; Pluger et al., 2000; see also Meera et al., 1996; Tanaka et al., 1997). Without the β1 subunit, BK channels do not respond adequately to the Ca^{2+} released in a spark, and consequently the β1 knock-out mice suffer from hypertension and cardiomegaly. Second, spark-STOC coupling in smooth muscle has emerged as an ideal system for the study of signaling within Ca^{2+} microdomains. The reason, in part, is that both the Ca^{2+} signal, i.e., the spark, and the activity of the Ca^{2+} target, the BK channels, can be monitored at high temporal resolution using imaging and patch-clamp technology, respectively. The mechanism of BK channel activation studied at this resolution may provide insight into the action of Ca^{2+} on other targets within a Ca^{2+} signaling microdomain.

Address correspondence to John V. Walsh, Jr, Department of Physiology, University of Massachusetts Medical Center, Worcester, MA 01655. Fax: (508) 856-5997; E-mail: john.walsh@umassmed.edu

*_Abbreviations used in this paper:_ RyR, ryanodine receptor; SR, sarcoplasmic reticulum; STOC, spontaneous transient outward current.

Published June 10, 2002

A critical factor in the generation of STOCs is the level of Ca^{2+} concentration ($[Ca^{2+}]$) sensed by the BK channels during a Ca^{2+} spark, but an experimental determination of this $[Ca^{2+}]$ is fraught with difficulties. An image-based determination of the $[Ca^{2+}]$ in the spark microdomain using a fluorescent Ca^{2+} indicator is problematical since the local Ca^{2+} and indicator do not necessarily come into equilibrium during the spark (Stern, 1992; Naraghi and Neher, 1997). Moreover, the relevant microdomain might encompass only a fraction of the smallest region which can be monitored optically, and hence the estimated $[Ca^{2+}]$, which will be an average for the entire region monitored, will be too low. Attempts to make estimates of the $[Ca^{2+}]$ based on a number of assumptions, for example the area of membrane occupied by the activated BK channels, have led to $[Ca^{2+}]$ values ranging from 300 nM to 100 μM (Nelson et al., 1995; Perez et al., 1999, 2001; ZhuGe et al., 1999).

We report here a new approach for determining the $[Ca^{2+}]$ that activates BK channels at the spark site. Our approach relies on a "signal mass" methodology for measuring the total amount of Ca^{2+} released during a spark from which the current flowing through RyRs ($I_{Ca(spark)}$) can be determined, a methodology which we developed previously (ZhuGe et al., 2000). We combine this with an analysis of the voltage dependence of the conductance for K^+ that is activated during the STOC, a quantity which we designate $g_{(STOC)}$. This conductance is then compared with the voltage dependence of BK channels at various $[Ca^{2+}]$s previously obtained in excised membrane patches (Singer and Walsh, 1987). We show that, during a Ca^{2+} spark, the BK channels causing an STOC are exposed to a mean $[Ca^{2+}]$ on the order of 10 μM. Such concentrations are at least an order of magnitude higher than the highest concentration of global Ca^{2+} that can be reached, which is ~1 μM for the cells employed here (Becker et al., 1989). The area of membrane over which BK channels are activated during a spark is estimated to be well under 1 μm^2. We also conclude that the BK channels are not distributed uniformly over the membrane of the entire cell but are found at high concentration at the spark site, with a lower density elsewhere. The method described here can readily be employed in other preparations which have STOCs.

MATERIALS AND METHODS

Isolation of Smooth Muscle Cells and Patch-clamp Recording

Single smooth muscle cells from the stomach muscularis of *Bufo marinus* were prepared by standard enzymatic dissociation as described (Fay et al., 1982). Membrane currents were recorded with a tight-seal, whole-cell patch configuration using an Axopatch 1D amplifier. The currents were low-pass filtered (200-Hz cutoff) then digitally sampled at 1 kHz and stored for analysis. The extracellular solution contained (in mM): NaCl 88, KCl 45, $CaCl_2$ 1.8, $MgCl_2$ 1, HEPES 10, pH adjusted to 7.4 with NaOH. Pipettes were filled with a solution containing (in mM): KCl 137, $MgCl_2$ 3, HEPES 10, Na_2ATP 3, fluo-3 0.05, and pH adjusted to 7.2 with KOH. All experiments were performed at room temperature. Events were counted as STOCs if they exceeded a threshold of 80 pS. The kinetics of events were analyzed with Excel using the equations in the legend of Fig. 1, after visual inspection to eliminate anomalies such as multiple events overlapping in time.

Imaging and Measurement of Ca^{2+} Sparks

Fluorescent images were obtained using fluo-3 as the calcium indicator and a custom-built, wide-field, high-speed digital imaging system which is described in detail elsewhere (ZhuGe et al., 2000). Briefly, rapid imaging was made possible by using a cooled high-sensitivity, charge-coupled device camera (128 × 128 pixels) developed in conjunction with the Massachusetts Institute of Technology Lincoln Laboratory. The imaging speed was 100 Hz, with a 10 ms exposure for each image. The camera was interfaced to a custom-made, inverted microscope equipped with a 40× oil immersion lens (NA 1.3); each pixel covered a 333- × 333-nm area of the cell. The 488-nm line of a multiline Argon laser provided fluorescence excitation for the indicator fluo-3, and a laser shutter controlled the exposure duration. Emission of the Ca^{2+} indicator was monitored at wavelengths >500 nm. To obtain a constant concentration of Ca^{2+} indicator, fluo-3 (50 μM) was delivered through the patch pipette, and measurements were not commenced until 10–15 min after disruption of the patch. After this time no significant change in background fluorescence was detected. Subsequent image processing and analysis were performed off-line using a custom-designed software package, running on a Silicon Graphics workstation.

Two measures of Ca^{2+} sparks were employed: the conventional fluorescence ratio, $\Delta F/F_0$, within a restricted volume; and the change in total fluorescence, $F^T - F^T{}_0$, over a larger volume, designated as the Ca^{2+} signal mass. These measurements have been described previously in detail (ZhuGe et al., 2000); a brief description follows. For the fluorescence ratio measure, the fluo-3 images, with pixel size 333 by 333 nm, were first smoothed by convolution with a 3 × 3 pixel approximation to a two-dimensional Gaussian ($\sigma = 1$). Fluorescence ratios were then calculated and expressed as a percentage on a pixel to pixel basis. The $\Delta F/F_0$ traces in the figures follow the time course of the single pixel that had the highest fluorescence ratio, that is, the brightest pixel, which we call the epicenter pixel of a given spark. The value of the second measure, the Ca^{2+} signal mass, for each spark was computed from the two-dimensional, wide-field fluorescence images of fluo-3 according to the equations:

$$\text{Total fluorescence, } F^T(t) = \sum_{\Delta x=-20}^{20}\sum_{\Delta y=-20}^{20}[F(x+\Delta x, y+\Delta y, t)].$$

$$\text{Signal mass, } sm(t) = G[F^T(t) - F^T(t0)].$$

The signal mass (sm[t]) is the product of the detector gain (G) times the change in total fluorescence (F^T) summed over a 13.7-μm square region (41 pixels on a side in the x-y plane), surrounding the spark epicenter pixel (x,y) as determined from the $\Delta F/F_0$ images. The number of moles of Ca^{2+} bound to fluo-3 was calculated by the equation: $\frac{2.44 \times sm(t)}{6.022 \times 10^{23}}$, where 2.44 is a calibration factor determined previously (ZhuGe et al., 2000). We have shown previously that the signal mass at each point in time until the peak is reached is directly proportional to the total amount of Ca^{2+} released into the cytosol from the onset of the spark up to that point in time. Thus, the rate of rise of the signal mass is

Downloaded from www.jgp.org on July 15, 2008

Published June 10, 2002

proportional to the Ca^{2+} current through RyRs during a Ca^{2+} spark, $I_{Ca(spark)}$.

Modeling of Spark and BK Channel Microdomain

To model the voltage- and $[Ca^{2+}]$-dependent activation of BK channels in an STOC, we first performed a series of spark simulations. Finite difference approximations were used to solve a set of partial differential equations for the reaction-diffusion kinetics in a cylindrical coordinate system and implemented using custom software as described previously (ZhuGe et al., 2000). Briefly, the cell was modeled as a circular cylinder with a radius of 3 μm, containing 50 μM fluo-3 (K_d = 1.1 μM, $k_{on} = 8 \times 10^{-7}$ $M^{-1}s^{-1}$, k_{off} = 90 s^{-1}, D = 22 $\mu m^2 s^{-1}$) and either 27 or 230 μM "fixed buffer" (K_d = 1 μM, $k_{on} = 10^{-8}$ $M^{-1}s^{-1}$, k_{off} = 100 s^{-1}), and with resting $[Ca^{2+}]$ = 100 nM. The spark event was modeled as a constant release of Ca^{2+} (D = 250 $\mu m^2 s^{-1}$) for a duration of 15 ms, the average spark duration for the cells in this study (ZhuGe et al., 2000). The spark current was modeled as 1 pA for the 27 μM fixed buffer simulation, and 3 pA for the 230 μM fixed buffer simulation. These values for the current were determined from the mean signal mass that we measured for a Ca^{2+} spark in an earlier study on the same cells employed here (ZhuGe et al., 2000). That is, we measured a mean Ca^{2+} signal mass whose rate of rise corresponded to a mean $I_{Ca(spark)}$ of 0.6 pA. Since the measured signal mass and hence $I_{Ca(spark)}$ will depend on the amount of fixed buffer, then the assumption of a greater amount of fixed buffer for a simulation demands that the underlying Ca^{2+} current be greater. Thus, the measurement of the Ca^{2+} signal mass places constraints on our choice of the values of $I_{Ca(spark)}$ and fixed buffer. For one set of simulations, 230 μM fixed buffer with the rate constants given was chosen, simply because that is the estimate published for smooth muscle (Bond et al., 1984). We also did another set of simulations using a relatively low concentration of fixed buffer (27 μM), because results of our earlier study suggested that the amount of fixed buffer is low (ZhuGe et al., 2000) and because this small amount of buffer made the simulation and modeling well behaved in the absence of fluo-3. The specific value of 27 μM also means that the rate of rise of the smallest measured mean signal mass corresponds to an $I_{Ca(spark)}$ of 0.35 pA, a value equal to a careful estimate of the single RyR current in physiological conditions (Mejia-Alvarez et al., 1999). The spark "site" was modeled as a small, cylindrically shaped volume, placed along the center axis of the cell at a distance of 25 nm from the flat end of the cylinder into which the Ca^{2+} was released. This spark site was itself 25 nm in height and had a diameter of either 60 nm for the 1 pA release or 104 nm for the 3 pA release. In this way the Ca^{2+} current density for the different simulations was held constant.

These spark simulations provided an estimate of the spatial distribution of the $[Ca^{2+}]$ immediately under the plasma membrane in the area surrounding the spark. We next modeled the voltage and $[Ca^{2+}]$ relationship of a single BK channel. The relationship between P_o and voltage was characterized previously for single BK channels from these cells (Singer and Walsh, 1987) and was well fit by the Boltzmann relationship:

$$P_o = [1 + e^{-K(V - V_{0.5})}]^{-1}, \quad (1)$$

where $V_{0.5}$ is the voltage where P_o = 0.5 and the logarithmic potential sensitivity K^{-1} was determined to be 11 mV. We employed a seventh-order polynomial to fit the nonlinear relationship between log $[Ca^{2+}]$ and $V_{0.5}$ (Meera et al., 1996; Wallner et al., 1999). By combining these two equations we were able to compute the (equilibrium) P_o for individual BK channels exposed to a given $[Ca^{2+}]$. Together with the $[Ca^{2+}]$ profiles from the spark simulations, we then were able to generate simulated voltage-$g_{(STOC)}$ data by assuming different physical distributions of BK channels across the plasma membrane. The BK channel distribution was modeled as uniformly distributed (equivalent to a uniform random distribution) and confined within a circular area of the plasma membrane centered opposite the Ca^{2+} release site which was placed at a distance of 25 nm normal to the plasma membrane. Finally, custom software was used to vary both the BK channel density and the size of this circular area from 18 nm to 3 μm to find the best (χ^2) fit to the observed $g_{(STOC)}$ data. The maximum radius of 3 μm was in fact equivalent to a uniform, ubiquitous distribution as the free $[Ca^{2+}]$ at this distance from the spark did not increase above the resting level.

Statistics

Data were presented as means ± SEM and were analyzed statistically with Student's *t* test.

RESULTS

The basic idea of the present study is to compare the K^+ conductance underlying an STOC ($g_{(STOC)}$) to the voltage dependence of the BK channels. In this way, as will be apparent below, we are able to determine the $[Ca^{2+}]$ to which the BK channels are exposed during a spark. We began by measuring $g_{(STOC)}$ at various membrane potentials. This is made possible by the fact that STOCs are pure K^+ currents since they are due to activation of BK channels. The evidence for this is that the STOCs are completely blocked by iberiotoxin (100 nM) (Nelson et al., 1995; ZhuGe et al., 1999), and the rate of their decay at 0 mV matches the mean open time of the BK channels in this preparation (ZhuGe et al., 2000). All the experiments reported here were performed in the whole-cell patch configuration, with E_K set at −28 mV ($[K^+]_o$ = 45 mM and $[K^+]_i$ = 137 mM). Under these conditions the unitary conductance for BK channels (γ) as studied in excised inside-out patches is constant over the range of voltages employed in the present study (Singer and Walsh, 1987). Hence, at equilibrium the following equation applies:

$$g_{(STOC)} = N \times P_{o(BK)} \times \gamma,$$

where N is the number of BK channels underlying the STOC, γ is the unitary conductance of the BK channels, and $P_{o(BK)}$ is the probability of the BK channels being open. This last is a function of both $[Ca^{2+}]$ and membrane potential, i.e.,

$$P_{o(BK)} = f(V_m, [Ca^{2+}]).$$

As noted, γ is a constant at the K^+ concentrations and over the range of voltages employed here, and N is also a constant at different voltages. Hence, $g_{(STOC)}$ reflects the P_o of the BK channels under these conditions. As shown below, the sparks do not change in magnitude as a function of voltage, and hence the

Downloaded from www.jgp.org on July 15, 2008

Published June 10, 2002

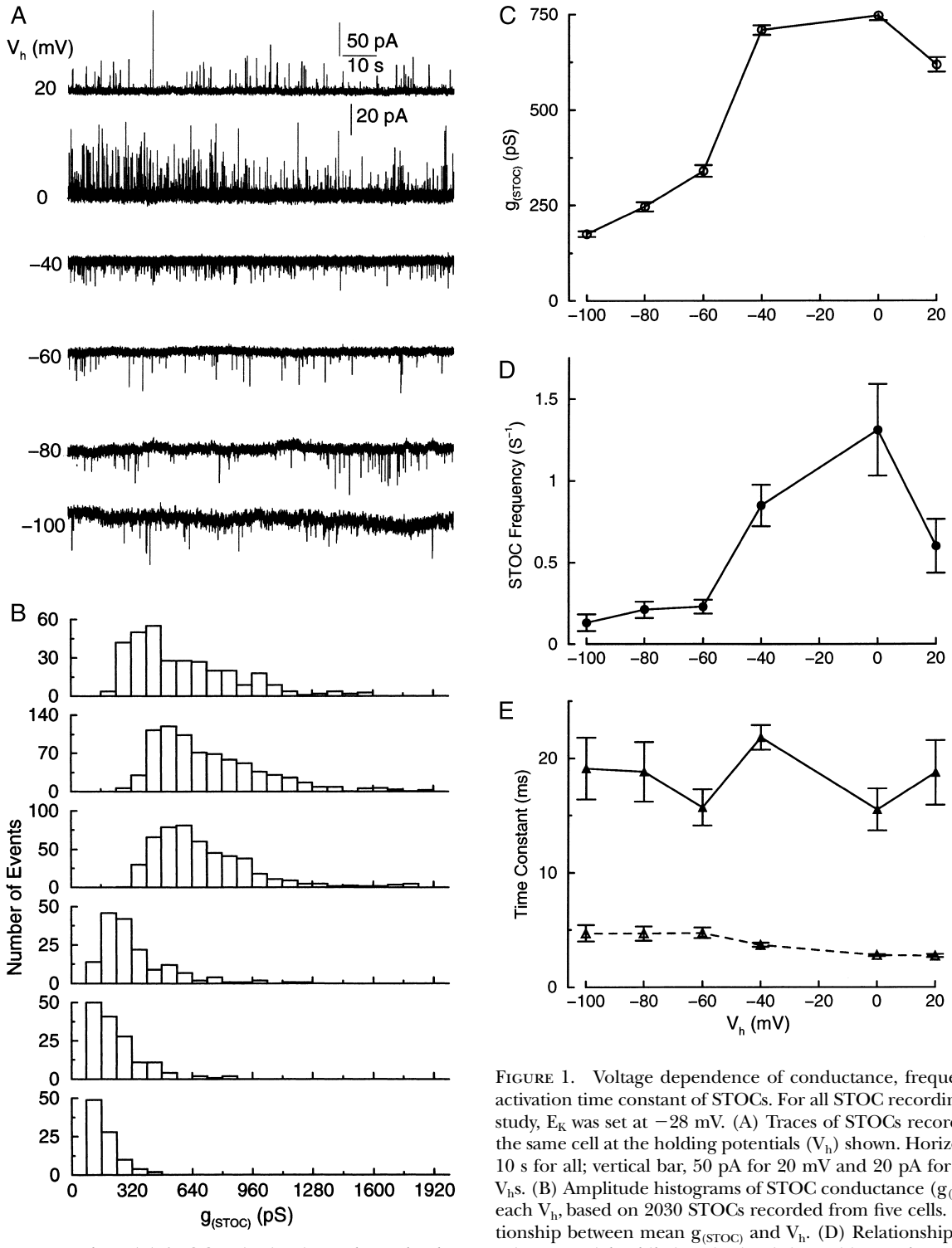

FIGURE 1. Voltage dependence of conductance, frequency, and activation time constant of STOCs. For all STOC recordings in the study, E_K was set at −28 mV. (A) Traces of STOCs recorded from the same cell at the holding potentials (V_h) shown. Horizontal bar, 10 s for all; vertical bar, 50 pA for 20 mV and 20 pA for all other V_hs. (B) Amplitude histograms of STOC conductance ($g_{(STOC)}$) for each V_h, based on 2030 STOCs recorded from five cells. (C) Relationship between mean $g_{(STOC)}$ and V_h. (D) Relationship between STOC frequency and V_h. (E) STOC activation is accelerated at less negative potentials while inactivation is insensitive to changes in voltage. Time constants for STOC activation (dashed line) were derived by fitting the activation phase with $I(t) = I_{max}[1 - \exp(-t/\tau)]^3$, where I_{max} is the peak current (ZhuGe et al., 2000). Time constants for STOC inactivation (solid line) were determined by fitting the decay phase with a single exponential.

$[Ca^{2+}]$ at the spark site remains constant at various potentials. Therefore, comparison of the $g_{(STOC)}$-V_m relationship to the family of P_o-V_m curves at different $[Ca^{2+}]$'s for the BK channels should provide information about the $[Ca^{2+}]$ at the cytosolic surface of the BK channels during a spark as well as insight into the spatial structure of the spark-STOC microdomain.

Downloaded from www.jgp.org on July 15, 2008

Published June 10, 2002

$g_{(STOC)}$ Is Smaller at More Negative Membrane Potentials

Fig. 1 A shows typical STOC traces obtained at the potentials indicated, with E_K at −28 mV as it was in all the experiments described here. The conductance for each STOC was determined as follows:

$$g_{(STOC)} = I_{BK}/(V_m + 28\ mV).$$

In Fig. 1 B, the distribution of values for $g_{(STOC)}$ at each of the six potentials is shown for all cells studied. It can be seen that the values decrease at more negative potentials with a sharp decline between −40 and −60 mV. The entire distribution appears to shift to the right at more positive potentials, the significance of which is considered below. Fig. 1 C shows the mean $g_{(STOC)}$ over a range of potentials for all the cells studied. As in Fig. 1 B, a sharp decrease in $g_{(STOC)}$ magnitude can be seen between −40 and −60 mV. It is also noteworthy that the magnitude of $g_{(STOC)}$ does not increase as the potential is increased from −40 to 20 mV. Fig. 1 D shows the frequency of the corresponding STOCs at each potential. Fig. 1 E shows the time constants for the rate of rise and decay of the STOCs over this range of potentials. The decay time constant does not change significantly over the range of potentials shown and corresponds approximately to the mean open time of the BK channels as measured in excised inside-out patches in the same cell type (Singer and Walsh, 1987).

The Magnitude of Ca^{2+} Sparks Does not Change as a Function of Potential

A possible reason for the decrease in $g_{(STOC)}$ at potentials more negative than −40 mV is that the amount of Ca^{2+} released from the SR during a spark decreases at negative potentials. We therefore examined Ca^{2+} sparks at 0 and −80 mV. The results are shown in Fig. 2. Fig. 2 A shows the temporal evolution of a typical Ca^{2+} spark, with images above and the traces indicating the fluorescence ratio and the signal mass below. Fig. 2 B, a, provides a histogram of the distribution of $\Delta F/F_o$ at 0 and −80 mV, and Fig. 2 B, c, does the same for the Ca^{2+} signal mass. Fig. 2 B, b, d, and e, compare the mean $\Delta F/F_0$, signal mass, and frequency at 0 and −80 mV. While spark frequency at 0 mV was greater, there was no difference in spark amplitude at 0 and −80 mV by either of the two measures of spark magnitude, $\Delta F/F_o$ or Ca^{2+} signal mass.

As we have shown previously (ZhuGe et al., 2000), the Ca^{2+} signal mass trace is the increase in total fluorescence which is proportional to the total amount of Ca^{2+} released during a spark as opposed to the Ca^{2+} concentration. The signal mass, expressed in terms of total charge, rather than total moles of Ca^{2+}, is equal to the product of the magnitude of $I_{Ca(spark)}$ and its duration, the latter corresponding to the time to peak of the signal mass. If the peak signal mass is the same at 0 and −80 mV, it would seem that the magnitude of $I_{Ca(spark)}$ must be the same; otherwise the two parameters, duration and magnitude of current, would have to change in precisely the opposite way to compensate for one another. In fact, we did not detect a significant difference in the time to peak for the signal mass at 0 and −80 mV; these values are 15 ± 2 ms and 14 ± 4 ms ($P > 0.07$), respectively. Thus, the values of $I_{Ca(spark)}$ and its duration are also the same at 0 and −80 mV. We conclude that the decrease in $g_{(STOC)}$ at negative potentials is not due to a difference in the Ca^{2+} sparks.

The $g_{(STOC)}$-V_m Relationship Corresponds Most Closely to the P_o-V_m Relationship for BK Channels in the Presence of 10 μM Ca^{2+}

Since the magnitude of the Ca^{2+} sparks does not change with membrane potential, the smaller magnitude of $g_{(STOC)}$ at negative potentials must be due to a decrease in P_o of the BK channels as a function of voltage at a given $[Ca^{2+}]$. For each $[Ca^{2+}]$, there is a characteristic P_o-V_m curve for the BK channels for smooth muscle cells. The P_o-V_m relationship for BK channels in the cell type used here has been studied previously in excised, inside-out patches (Singer and Walsh, 1987) and is in agreement with those found in other smooth muscle preparations (Carl et al., 1996). This Ca^{2+} sensitivity reflects the presence of the β1 subunit, which appears to be characteristic of BK channels in smooth muscle cells (Tanaka et al., 1997). Three such curves for BK channels in the same cell type at 100 μM, 10 μM, and 1 μM Ca^{2+} (Singer and Walsh, 1987) are shown in Fig. 3 A along with the $g_{(STOC)}$-V_m curve from Fig. 1. The shaded area shows the variation that was observed at 10 μM Ca^{2+}. This variation resulted only in a shift of the curve along the x-axis without a change in the slope factor (Singer and Walsh, 1987). The mean $V_{0.5}$ at 10 μM is the same as that found for the cloned α and β1 subunits of the BK channel from human smooth muscle coexpressed at a 1:1 ratio in *Xenopus* oocytes (Meera et al., 1996).

The values for P_o in the plots of Fig. 3 A are equilibrium values, but are the values for $g_{(STOC)}$ obtained under conditions where the BK channels approach equilibrium with the cytosolic Ca^{2+} caused by the spark? This appears to be the case as shown by the following considerations. As we have demonstrated previously, the $[Ca^{2+}]$ within the spark microdomain rises quickly and abruptly at the onset of the spark, either reaching a plateau level within 1–2 ms or rising relatively slowly for the duration of the spark current, ~15 ms on average (ZhuGe et al., 2000, Fig. 11). The question is whether the STOCs rise to a plateau level within this 15 ms, indicating that the BK channels have neared equilibrium

Downloaded from www.jgp.org on July 15, 2008

Published June 10, 2002

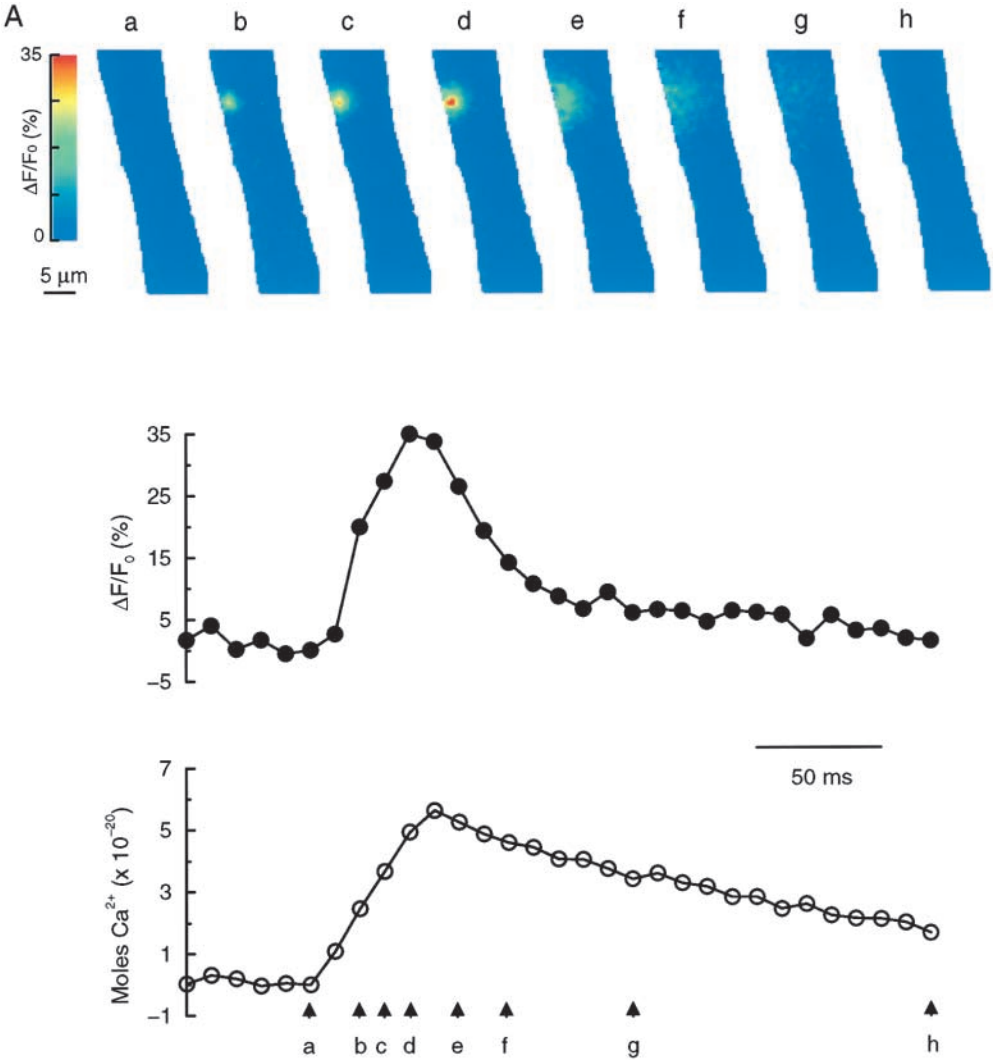

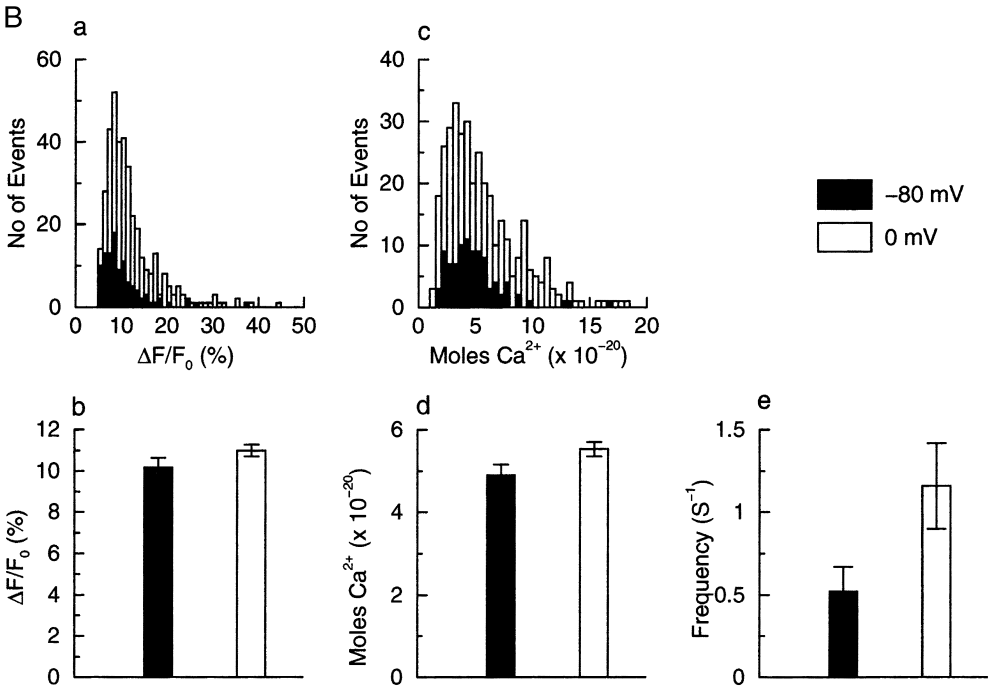

FIGURE 2. Ca^{2+} sparks recorded at −80 and 0 mV are of the same amplitude. (A) An example of a Ca^{2+} spark acquired at −80 mV in the presence of 1.8 mM extracellular Ca^{2+}. Images show the spatial and temporal evolution of the Ca^{2+} spark. Top trace, the time course of change in fluorescence in the pixel (333 nm × 333 nm) where the peak fluorescence is reached, i.e., the epicenter pixel. Bottom trace, for the same spark, time course of Ca^{2+} signal mass, that is the total fluorescence for a volume subtended by an area 41 pixels on a side in the x-y plane and centered on the epicenter pixel. The signal mass is proportional to the total amount of Ca^{2+} released by the spark (see ZhuGe et al., 2000). (B, a) Amplitude histogram of Ca^{2+} sparks recorded at −80 and 0 mV and (b) their means. (c) Signal mass histogram of Ca^{2+} sparks recorded at −80 and 0 mV and (d) their means. (e) Mean frequency of Ca^{2+} sparks at −80 and 0 mV.

Downloaded from www.jgp.org on July 15, 2008

Published June 10, 2002

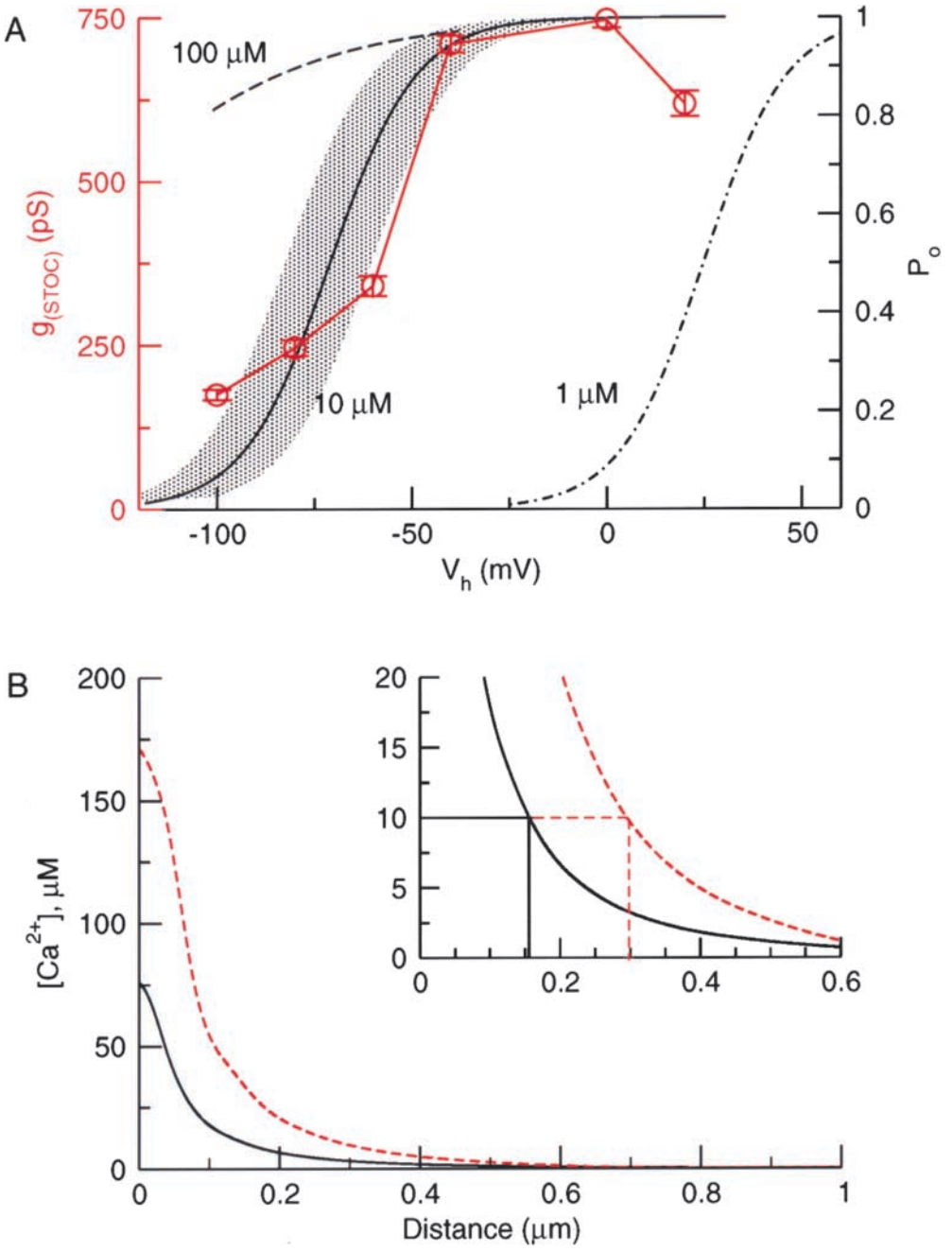

FIGURE 3. (A) Relationship between voltage dependence of $g_{(STOC)}$ and P_o for BK channels. Red curve (continuous line connecting circles) is plot of $g_{(STOC)}$ as a function of holding potential based on the experiments in Fig. 1. Three black lines (dot-dashed, solid, and dashed) were drawn according to published data on P_o of BK channels in excised inside-outside patches exposed to 1, 10, and 100 μM $[Ca^{2+}]$ in the same cell type (Singer and Walsh, 1987). The shaded area indicates the variation observed at 10 μM. As in the cited publication, the data are fit according to the Boltzmann relationship (Eq. 1). (B) Simulation of $[Ca^{2+}]$ spatial profile at the end of 15-ms pulses of 1 pA of Ca^{2+} current from the RyRs during a spark (50 μM fluo-3 plus 27 μM fixed buffer; black solid line) and 3 pA (50 μM fluo-3 plus 230 μM fixed buffer; red dashed line). Inset is the same plot on an expanded scale. The inset provides an indication of the lateral distance from the Ca^{2+} release site where the $[Ca^{2+}]$ reaches 10 μM in the two buffer conditions.

with the cytosolic $[Ca^{2+}]$ over the entire range of potentials employed here. Using the time constants in Fig. 1 E and the expression in the legend to Fig. 1, we found that the STOCs rise to 99.5% of their plateau value at 0 mV and 86% at −80 mV. (As can be seen in Fig. 1 E, the time constant for the rise of the STOCs is increased perceptibly as the potential drops from 0 to −60 mV, with little change over the range of −60 to −100 mV. The time constant of STOC decay shows no systematic change as a function of potential.) From these quantitative considerations, the BK channels appear to be close to equilibrium with the Ca^{2+} in the spark microdomain by the time the spark Ca^{2+} current terminates. Moreover, from a qualitative point of view, we note that correction for the slower rate of rise as the potential is made more negative will shift the $g_{(STOC)}$-Vm curve of Fig. 3 A to the left, bringing it closer to the $P_{o(BK)}$-V_m curves for $[Ca^{2+}]$s >10 μM. Thus, the estimates we make for the $[Ca^{2+}]$ sensed by the BK channel may be somewhat below the actual ones.

The data in Fig. 3 A lead us to conclude that the BK channels contributing to an STOC are exposed to a $[Ca^{2+}]$ on the order of 10 μM. (An upper limit is placed on this concentration by the fact that the free $[Ca^{2+}]$ in the SR is ~150 μM [ZhuGe et al., 1999].)

Downloaded from www.jgp.org on July 15, 2008

Published June 10, 2002

The Spatial Profile of [Ca^{2+}] in the Spark Microdomain Derived from Measures of $I_{Ca(spark)}$

The signal mass (Fig. 2 A) provides a measure of the total amount of Ca^{2+} or the total charge carried by Ca^{2+} that is released during a spark. A trace of the signal mass, like that shown in Fig. 2 A, provides a time-integrated index of the Ca^{2+} or charge released; hence the derivative of its rising phase provides a measure of the Ca^{2+} current through the RyR's during a spark or $I_{Ca(spark)}$ (ZhuGe et al., 2000). The mean duration of $I_{Ca(spark)}$ was found to be ~15 ms. Using this value and the value for $I_{Ca(spark)}$, the spatial profile of [Ca^{2+}] can be calculated at the end of the 15-ms period, a time when the STOC is at its peak amplitude. Here we are referring to the lateral extent of the [Ca^{2+}] profile along the plasma membrane as we proceed outward from the Ca^{2+} release site. For these calculations we place the Ca^{2+} release site 25 nm from the plasma membrane, in accord with measures of the distance from the SR membrane to the plasma membrane in smooth muscle cells (Somlyo and Franzini-Armstrong, 1985). However, both the actual magnitude of $I_{Ca(spark)}$, as determined by the signal mass method, and its spatial extent depend on the Ca^{2+} buffers in the cell. That is, with more buffering the slope of the signal mass must be multiplied by a greater proportionality constant to obtain the actual magnitude of the $I_{Ca(spark)}$ (ZhuGe et al., 2000). Fig. 3 B shows the spatial profile of [Ca^{2+}] for two conditions: 50 μM fluo-3 as the sole mobile buffer with a uniform concentration, either 27 or 230 μM, of fixed buffer with a K_d of 1 μM. The former condition (27 μM) is one where the fluo-3 dominates and the latter (230 μM) is the one estimated for smooth muscle (Bond et al., 1984). (For reasons discussed below, it appears that this estimate of fixed buffer constitutes a maximum.) Fig. 3 B indicates that the radius of the region where [Ca^{2+}] is ≥10 μM is ~150 nm (area = 0.07 μm^2) or 300 nm (area = 0.28 μm^2) for the two buffer conditions. (For comparison, at a [Ca^{2+}] equal to 2 μM, the radius is equal to 380 and 540 nm for the low and high buffer conditions, respectively.)

The Areas Containing the BK Channels Activated by a Spark Are Homogenous in their Spatial Extent

The following considerations suggest that the areas over which BK channels are activated during a spark make up a single population. Fig. 1 B indicates that there are not several qualitatively different types of microdomains containing the activated BK channels, those large in area and those quite restricted in area. The latter would have RyRs and BK channels necessarily closer since they lie in a more restricted space. In this case one might imagine that the small conductances observed at potentials of −80 and −100 mV in Fig. 1 B are due to a class of STOC domains that are of lesser spatial extent. If this were the case, then upon raising the potential to more positive levels, these small conductances would not disappear. Rather, they would remain as one of two or more peaks in the distributions of Fig. 1 B at potentials positive to −80 mV. However, such a multimodal distribution is not seen, and so heterogeneity of this sort does not appear to exist. To a first approximation, the areas containing the activated BK channels appear to be normally distributed. The small conductances that remain at the very negative potentials (Figs. 1 B and 3 A) appear to be due to the BK channels closest to the RyRs at the spark site. (Such homogeneity does not, however, mean that the spark microdomain is a highly stereotyped arrangement. We have demonstrated in earlier work that the ratio of RyRs to BK channels varies among sparks [ZhuGe et al., 2000] and among spark sites [unpublished data].

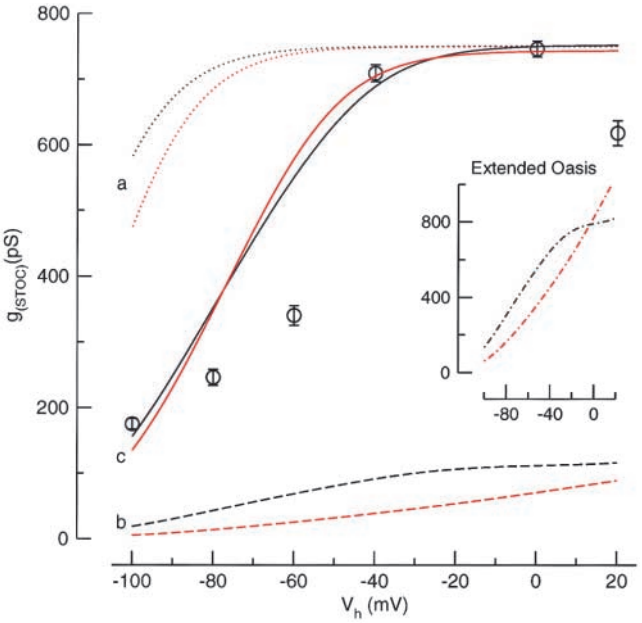

FIGURE 4. Simulations indicating that voltage dependence of $g_{(STOC)}$ is best explained by a model with an oasis of BK channels which sense a mean [Ca^{2+}] on the order of 10 μM. The simulation of a "handshake" model is shown by lines "a" (dotted lines), uniform density of BK channels by lines "b" (dashed lines), and an oasis of BK channels by lines "c" (solid lines). The inset shows the results for an "extended oasis" model. Each of these models is described in the text. The two lines for each model correspond to two concentrations of fixed buffer, 27 μM (red lines) or 230 μM (black lines). For case "a," the BK channels lie directly opposed to the RyRs, giving areas with a radius of 30 nm for the 27 μM buffer and 52 nm for the 230 μM. (The larger radius for the latter simulation results from the fact that $I_{Ca(spark)}$ is larger in the latter case, with the density, $I_{Ca(spark)}/\mu m^2$, kept constant.) For case "b," the BK channels extended at a constant density for an "indefinite extent," which we took to be 3 μm. For case "c," the simulation converged on an area with a radius of 250 nm for 27 μM buffer and 450 nm for 230 μM buffer. In each case the Ca^{2+} release site (i.e., the RyRs) are located at a distance 25 nm from the plasma membrane. The details of the simulations are described in the MATERIALS AND METHODS.

Downloaded from www.jgp.org on July 15, 2008

Published June 10, 2002

Hence, at any spark site the ratio of RyRs to BK channels can vary considerably.)

DISCUSSION

The results reported above can be summarized as follows. First, the Ca^{2+} sparks do not change in magnitude or time course as a function of membrane potential, though they do increase in frequency at more positive potentials. Second, the magnitude of $g_{(STOC)}$ remains fairly constant at potentials ranging from −40 to 0 mV and declines steeply at more negative potentials. Interestingly, this means that the number of BK channels activated by a spark remains roughly constant from −40 mV (the region of resting potential) to 0 mV. Third, the BK channels underlying an STOC are exposed to a $[Ca^{2+}]$ on the order of 10 μM during a Ca^{2+} spark. Fourth, the membrane area enclosing a region with a $[Ca^{2+}] \geq 10$ μM at a spark site has a lateral radius on the order of 150–300 nm (area = 0.07–0.28 μm^2), this determination depending on the precise character of the fixed Ca^{2+} buffers in the cell. Fifth, the areas containing activated BK channels seem to constitute a single population rather than multiple populations with different mean areas. Further insight into these conclusions was obtained from simulations discussed in the following sections. The simulations lead to the conclusion that the BK channels are not uniformly distributed over the plasma membrane but are clustered into regions of higher than average density at the spark sites.

Simulations of Ca^{2+} Sparks and STOCs Are Consistent with an "Oasis" Model of BK Channels Concentrated in the Spark Microdomain, but not with a "Handshake" Model or a Uniform Distribution of BK Channels

Using spatial profiles of $[Ca^{2+}]$ shown in Fig. 3 B and curves relating $P_{o(BK)}$ to $[Ca^{2+}]$ and V_m of the sort shown in Fig. 3 A, the relationship between $g_{(STOC)}$ and V_m can be predicted by simulation using different models of BK channel distribution at the spark site. The results of such simulations are shown in Fig. 4 for three different models of spatial distribution of BK channels. We emphasize that these simulations are meant only to predict the general shape of the $g_{(STOC)}$-V_m relationship as shown by the open circles of Fig. 3 A which are also shown in Fig. 4.

The "Handshake" Model

The curves marked "a" in Fig. 4 show the expected relationship if each BK channel lies within 20 nm of a RyR as might be expected if the two molecules are in physical contact or are coupled by an adaptor protein. (There are two curves in each case, one for each of the buffering conditions shown in Fig. 3 B.) This might be dubbed a "handshake" model. Clearly, the plot for this model lacks the sharp decline in the region of −40 to −60 mV that characterizes the actual data given by the open circles. The inadequacy of the "handshake" model is reinforced by another consideration. The frequency of sparks at −80 mV is ∼45% that at 0 mV (Fig. 2 E), whereas the relative STOC frequency is 16% (Fig. 1 C). The decline in spark frequency appears to be due to the fact that, as in cardiac muscle, Ca^{2+} influx through voltage-activated Ca^{2+} channels can elicit sparks (Cannell et al., 1995; Lopez-Lopez et al., 1995; Arnaudeau et al., 1997; ZhuGe et al., 1998b), but these Ca^{2+} channels are essentially silenced at −80 mV (ZhuGe et al., 1998b). Hence, only a portion of the decline in STOC frequency is due to the decline in spark frequency. The remainder of this decline must be due to the decreased probability of BK channel opening, which leads either to failure of STOC generation or an STOC amplitude that is not detectable. If the decrease in STOC frequency matched the decrease in the spark frequency at very negative potentials, then the "handshake" model would apply. One cautionary note about the exclusion of the "handshake model" deserves mention. Our estimate of $[Ca^{2+}]$ is a lower limit for the reasons outlined in RESULTS, although it seems unlikely that the estimate could be an order of magnitude too low (Fig. 3 A). Furthermore, though it appears that a direct contact between the BK channels and the RyRs is unlikely, it is conceivable that the two may be linked by a series of scaffolding proteins that span a large distance.

Uniform BK Channel Density throughout the Cell Membrane

The curves marked "b" in Fig. 4 indicate the results to be expected if there is a uniform density of BK channels everywhere in the plasma membrane. The channel density is critical in determining these curves, with higher densities, bringing the curves of "b" closer to the actual data given by the open circles. We have estimated the density of BK channels in the smooth muscle cell type employed here to be $\sim 1/\mu m^2$ (Singer and Walsh, 1987), and we used this estimate to generate the curves of "b." Clearly the data of Fig. 3 A do not fit these curves.

In other smooth muscle types, determination of the density has yielded values of $2/\mu m^2$ for rabbit jejunum (Benham and Bolton, 1986) and rat cerebral artery (Perez et al., 2001) and $4/\mu m^2$ for human coronary artery (Tanaka et al., 1997). These differences appear to result from differences among cell types, with cells having higher mean density also generating larger STOCs. For example, in rat cerebral artery (Perez et al., 2001), the mean BK channel density is twice that observed here, but the STOCs comprise current from ∼18 BK channels, ∼3 times the number in the preparation employed here. This would seem to require an even higher degree of concentration of BK channels at a spark site. However, even if the highest estimate of BK

Downloaded from www.jgp.org on July 15, 2008

Published June 10, 2002

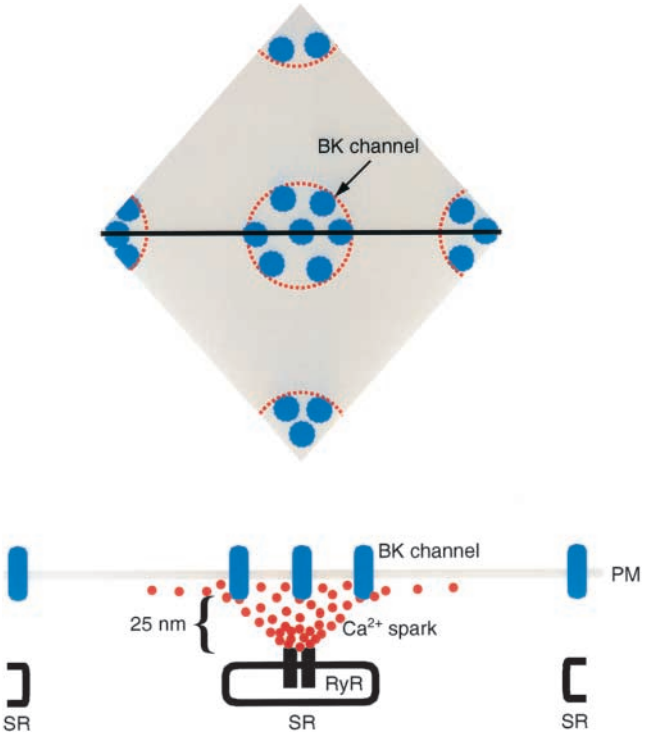

FIGURE 5. The "oasis" model of the spark-STOC microdomain. Top panel, the view of the BK channel distribution pattern as seen from the membrane surface. In the case of the oasis model, the channels at the spark site are confined to a region within the dotted circle. This region is less than one square micron in area (see text). In the case of the "extended oasis" model, there would be a ring of BK channels lying just outside the dotted circle (not depicted), which would not be activated by a Ca^{2+} spark. Bottom, cross-sectional view of the region marked by the black solid line in the top panel. Note that the distance between release site and plasma membrane is 25 nm. These depictions are qualitative representations and not drawn to scale.

channel density ($4/\mu m^2$) is employed in the simulations, a "best case" for the uniform distribution model, the curves do not match the $g_{(STOC)}$ data. In this case, the black curve plateaus at a value of ~447 pS at 0 mV, as compared with the actual value of 760 pS. And the red curve does not plateau at all, but is concave upward with no plateau. Hence, a model of uniform distribution does not match the $g_{(STOC)}$ data.

The Oasis Model: High Density of BK Channels in the Spark Microdomain

The curves marked "c" belong to a set of simulations where the BK channels exist at a uniform density within a certain lateral distance from the $[Ca^{2+}]$ release site along the membrane. Beyond this region the BK channel density falls to a negligible level. This is termed an "oasis" model. Given the dual constraints of the influence of $[Ca^{2+}]$ and V_m on the BK channel P_o, the simulation is designed to converge on an area for the oasis and a density for the BK channels which best fit the $g_{(STOC)}$ data. The plots resulting from this simulation match the general shape of the plot for the actual data shown in circles, i.e., flat at the more positive potentials, with a steep decline in the region of −40 to −60 mV and a failure to reach zero even at a potential of −100 mV. The curves "c" limit the extent of BK channels to an area of 250-nm radius for the low $I_{Ca(spark)}$ and buffering condition (red), and 450 nm for the high $I_{Ca(spark)}$ and buffering condition (black). For the 250-nm radius (area = 0.20 μm^2), the mean $[Ca^{2+}]$ in the oasis is 12.3 μM and the $[Ca^{2+}]$ at the oasis periphery is 5.5 μM; the mean number of BK channels is 5.3 and the BK channel density in the oasis is 26.5 channels/μm^2. For the 450-nm oasis (area = 0.64 μm^2), the mean $[Ca^{2+}]$ is 16.4 μM and the $[Ca^{2+}]$ at the oasis periphery is 4 μM; the mean number of BK channels is 5.4 and the BK channel density in the oasis is 8.4 channels/μm^2. Since we do not know the precise disposition of the BK channels or the RyRs within the oasis or the exact nature and spatial disposition of the fixed buffers, we can expect these simulations to correspond to the actual data only in an approximate way. Finally, we note that for the oasis model the fit to the data does not depend on the nonlinear relationship between $V_{0.5}$ and log $[Ca^{2+}]$ used for these simulations (Meera et al., 1996). If instead a linear relationship is employed (Carl et al., 1996), the fit to the actual data is somewhat better and the oasis shrinks to a radius of 150 and 350 nm for the low and high $I_{Ca(spark)}$ conditions, respectively.

An alternative to the oasis model is a "fortress" model in which there is a uniform density of BK channels everywhere in the plasma membrane but a physical barrier to Ca^{2+} movement at the same location as the periphery of the oasis. One such barrier could simply be a membrane or other wall-like structure. However, an effective barrier to ion diffusion must act as a barrier to K^+ and hence should appear as a series resistance for the K^+ current of the STOCs. In this case the reversal potential for STOCs should deviate from E_K, but in fact the reversal potential follows E_K quite closely (Fig. 1; see also Benham and Bolton, 1986). Moreover, for such a model to match the $g_{(STOC)}$ data, the mean channel density has to be almost an order of magnitude greater than what is estimated. Hence, it does not appear that the fortress model can be correct.

An Extended Oasis of BK Channels Larger than the Zone of BK Channel Activation

A second version of the oasis model will also yield a fit to the $g_{(STOC)}$ data. Like the oasis model described in the previous section, a high local density of BK channels is required. But unlike the above model, the oasis is larger than the zone of channel activation. Thus, an oasis of BK channels at higher than average density re-

Downloaded from www.jgp.org on July 15, 2008

Published June 10, 2002

mains, but within it there is a zone of activated BK channels. The results of simulations using this formulation yield the results given by the inset to Fig. 4. In this case the simulation matches the $g_{(STOC)}$ data only for high level of $I_{Ca(spark)}$ and buffer (black curve, inset) and not for the low level (red curve, inset), which unlike the $g_{(STOC)}$ data exhibits no plateau at potentials positive to −60 mV. The simulation yields a density of 8 BK channels/μm^2 within the oasis. With this model it is not necessary to revise upward the estimate of total number of BK channels per cell (or the mean density over the cell) since a high density of BK channels is only required up to the limit of the zone of activation. The size of the oasis is unspecified in this model, but the zone of activation is defined and sets a lower limit on the size of the oasis.

What then is the size of the zone of activated BK channels within such an extended oasis? The zone of activation will depend on the membrane potential, expanding at more positive potentials and constricting at more negative potentials. Hence, for example, at −40 mV, often used as an estimate of resting potential, 95% of the conductance in an STOC will come from a zone with a radius of 470 nM (area = 0.7 μm^2) over which the mean $[Ca^{2+}]$ is 15 μM, and the $[Ca^{2+}]$ at the periphery is 3.6 μM. At 0 mV, 95% of the conductance in an STOC will come from a zone of 490 nm (area = 0.75 μm^2) with a mean $[Ca^{2+}]$ of 14 μM and a peripheral $[Ca^{2+}]$ of 3.4 μM. This set of values is not much different at the two potentials, 0 and −40 mV, as might be expected from the fact that the value for $g_{(STOC)}$ is unchanged at the two potentials. At −80 mV, the values are: radius, 390 nm (area = 0.73 μm^2) from which 95% of the STOC conductance derives; mean $[Ca^{2+}]$, 21 μM; peripheral $[Ca^{2+}]$, 4 μM. Fig. 5 provides a depiction of the oasis and extended oasis models.

Ca^{2+} Sparks Do not Change as a Function of Membrane Potential

We find that the Ca^{2+} sparks as measured by $\Delta F/F_0$, signal mass, duration, and magnitude of $I_{Ca(spark)}$ are all unchanged at 0 and −80 mV; the frequency, however, is greater at 0 mV than at −80 mV. This is consistent with our measurements of free $[Ca^{2+}]$ in the SR which is the same at 0 and −80 mV (ZhuGe et al., 1998b). Also in cardiac and skeletal muscle the frequency, but not the magnitude, of Ca^{2+} sparks changes as a function of membrane potential (Klein et al., 1997; Collier et al., 1999). The constancy of spark magnitude over a range of membrane potentials has also been reported in portal vein smooth muscle (Arnaudeau et al., 1997). However, there is a single report in bladder smooth muscle that Ca^{2+} sparks measured by $\Delta F/F_0$ are greater in amplitude at more positive potentials (Herrera et al., 2001). There are two possible reasons for this finding. First and most likely, there may be differences in this regard in different smooth muscle cell types. Or second, if the region of measurement for a Ca^{2+} spark is too large, then at more positive potentials where the spark frequency is greater, several sparks might coalesce and appear as one.

Spatial Separation of Spark Sites Prevents Sparks from Becoming Global Increases in $[Ca^{2+}]$

The location of BK channels in oases separate from one another suggests that the RyRs causing sparks sites might be similarly arranged. At least one previous study suggests clustering of RyRs in adult vascular smooth muscle cells (Gollasch et al., 1998). Our results indicate that the Ca^{2+} from a spark arising at one STOC oasis cannot activate BK channels at a nearby oasis. Like the BK channels at potentials close to 0 mV, the RyRs have a K_d of ∼1 μM Ca^{2+} (Bezprozvanny et al., 1991). Hence, we would expect that Ca^{2+} sparks would not trigger Ca^{2+} waves. And indeed we do not see the generation of Ca^{2+} waves by sparks in these smooth muscle cells. In general, if sparks are to cause relaxation in smooth muscle cells, then they must not cause Ca^{2+} waves since the waves would elevate global $[Ca^{2+}]$ and initiate contraction. Spatially isolated oases of RyRs and BK channels appear to be a way of ensuring that the Ca^{2+} sparks will cause relaxation without triggering contraction.

The Spark Microdomain: a Summary

In all of the simulations which fit the $g_{(STOC)}$ data, the mean $[Ca^{2+}]$ sensed by the BK channels in the spark microdomain is on the order of 10 μM (range: 12–21 μM). The mean radius over which BK channel activation occurs may range from 250 nm (area = 0.2 μm^2) to 490 nm (area = 0.75 μm^2), depending on the fixed buffers, the magnitude of $I_{Ca(spark)}$, and in the case of the extended oasis model, the membrane potential. The values for mean $[Ca^{2+}]$ and spatial extent of BK channel activation provided by the simulations above are in excellent agreement with estimates from a simple qualitative examination of Fig. 3, A and B. Whereas the values for the mean area containing activated BK channels are only a fraction of one square micron, the mean spatial extent at full-width, half max (FWHM) in images like those in Fig. 2 is 2.7 μm. Hence, the FWHM does not seem to be a meaningful measure of the extent of the spark-STOC microdomain, and its use leads to an overestimate of the area of BK channel activation. In summary, the spark-STOC microdomain is a genuine microdomain with an area which is a fraction of one square micron, allowing the mean $[Ca^{2+}]$ to rise to ∼10 μM.

The simulations above also demand that the BK channels exist at higher than average density at the spark sites. There have been previous indications that

Downloaded from www.jgp.org on July 15, 2008

the BK channels are not uniformly distributed. Xiong et al. (1992), using portal vein smooth muscle and, more recently, Ohi et al. (2001), using vas deferens and bladder smooth muscle, have found evidence for clustering of BK channels based on activity of a high density of BK channels recorded in some patches of smooth muscle membrane excised with some SR apparently attached.

Meera et al. (1996) have called attention to the fact that the BK channel behaves as a "switch" operated by Ca^{2+}. At $[Ca^{2+}]$ below 1 μM, the channels are in the closed state at all physiological membrane potentials. At $[Ca^{2+}]$ of ≥10 μM the channels are in the open state over the range of physiological potentials. Since global $[Ca^{2+}]$ generally remains at levels <1 μM, the channels must be located within a microdomain where $[Ca^{2+}]$ reaches levels >1 μM for the switch to function reliably. As we have shown here, the spark microdomain satisfies this demand and provides a highly localized region where Ca^{2+} rises to a sufficient concentration to operate the BK channel switch.

We thank Lawrence Lifshitz and Michael Stern for helpful comments on the manuscript and Jeffrey Carmichael for excellent technical assistance.

This study was supported by a grant from the National Institutes of Health (HL61297) and by grants from the National Science Foundation (DBI-9724611 and DIR9200027).

Submitted: 31 January 2002
Revised: 12 April 2002
Accepted: 6 May 2002

REFERENCES

Arnaudeau, S., F.X. Boittin, N. Macrez, J.L. Lavie, C. Mironneau, and J. Mironneau. 1997. L-type and Ca^{2+} release channel-dependent hierarchical Ca^{2+} signaling in rat portal vein myocytes. *Cell Calcium.* 22:399–411.

Becker, P.L., J.J. Singer, J.V. Walsh, Jr., and F.S. Fay. 1989. Regulation of calcium concentration in voltage-clamped single smooth muscle cells. *Science.* 244:211–214.

Benham, C.D., and T.B. Bolton. 1986. Spontaneous transient outward currents in single visceral and vascular smooth muscle cells of rabbit. *J. Physiol.* 381:385–406.

Bezprozvanny, I., J. Watras, and B.E. Ehrlich. 1991. Bell-shaped calcium-response curves of $Ins(1,4,5)P_3$- and calcium-gated channels from endoplasmic reticulum of cerebellum. *Nature.* 351:751–754.

Bolton, T.B., and D.V. Gordienko. 1998. Confocal imaging of calcium release events in single smooth muscle cells. *Acta Physiol. Scand.* 164:567–575.

Bond, M., H. Shuman, A.P. Somlyo, and A.V. Somlyo. 1984. Total cytoplasmic calcium in relaxed and maximally contracted rabbit portal vein smooth muscle. *J. Physiol.* 357:185–201.

Brenner, R., G.J. Perez, A.D. Bonev, D.M. Eckman, J.C. Kosek, S.W. Wiler, A.J. Patterson, M.T. Nelson, and R.W. Aldrich. 2000. Vasoregulation by the β1 subunit of the calcium-activated potassium channel. *Nature.* 407:870–876.

Brown, D.A., A. Constanti, and P.R. Adams. 1983. Ca-activated potassium current in vertebrate sympathetic neurones. *Cell Calcium.* 4:407–420.

Cannell, M.B., H. Cheng, and W.J. Lederer. 1995. The control of calcium release in heart muscle. *Science.* 268:1045–1049.

Carl, A., H.K. Lee, and K.M. Sanders. 1996. Regulation of ion channels in smooth muscles by calcium. *Am. J. Physiol.* 271:C9–C34.

Collier, M.L., A.P. Thomas, and J.R. Berlin. 1999. Relationship between L-type Ca^{2+} current and unitary sacrcoplasmic reticulum Ca^{2+} release events in rat ventricular myocytes. *J. Physiol.* 516: 117–128.

Fay, F.S., R. Hoffman, S. Leclair, and P. Merriam. 1982. Preparation of individual smooth muscle cells from the stomach of *Bufo Marinus*. *Methods Enzymol.* 85:284–291.

Gollasch, M., G.C. Wellman, H.J. Knot, J.H. Jaggar, D.H. Damon, A.D. Bonev, and M.T. Nelson. 1998. Ontogeny of local sarcoplasmic reticulum Ca^{2+} signals in cerebral arteries: Ca^{2+} sparks as elementary physiological events. *Circ. Res.* 83:1104–1114.

Herrera, G.M., T.J. Heppner, and M.T. Nelson. 2001. Voltage dependence of the coupling of Ca^{2+} sparks to BK_{Ca} channels in urinary bladder smooth muscle. *Am. J. Physiol.* 280:C481–C490.

Kirber, M.T., E.F. Etter, K.A. Bellve, L.M. Lifshitz, R.A. Tuft, F.S. Fay, J.V. Walsh, Jr., and K.E. Fogarty. 2001. Relationship of Ca^{2+} sparks to STOCs studied with 2D and 3D imaging in feline oesophageal smooth muscle cells. *J. Physiol.* 531:315–327.

Klein, M.G., A. Lacampagne, and M.F. Schneider. 1997. Voltage dependence of the pattern and frequency of discrete Ca^{2+} release events after brief repriming in frog skeletal muscle. *Proc. Natl. Acad. Sci. USA.* 94:11061–11066.

Lopez-Lopez, J.R., P.S. Shacklock, C.W. Balke, and W.G. Wier. 1995. Local calcium transients triggered by single L-type calcium channel currents in cardiac cells. *Science.* 268:1042–1045.

Meera, P., M. Wallner, Z. Jiang, and L. Toro. 1996. A calcium switch for the functional coupling between α (*hslo*) and β subunits ($K_{V,Ca}\beta$) of maxi K channels. *FEBS Lett.* 382:84–88.

Mejia-Alvarez, P., R.C. Kettlun, E. Rios, M.D. Stern, and M. Fill. 1999. Unitary Ca^{2+} currents through cardiac ryanodine receptors under quasi-physiological ionic conditions. *J. Gen. Physiol.* 113:177–186.

Mironneau, J., S. Arnaudeau, N. Macrez-Lepretre, and F.X. Boittin. 1996. Ca^{2+} sparks and Ca^{2+} waves activate different Ca^{2+}-dependent ion channels in single myocytes from rat portal vein. *Cell Calcium.* 20:153–160.

Naraghi, M., and E. Neher. 1997. Linearized buffered Ca^{2+} diffusion in microdomains and its implications for calculation of $[Ca^{2+}]$ at the mouth of a calcium channel. *J. Neurosci.* 17:6961–6973.

Nelson, M.T., H. Cheng, M. Rubart, L.F. Santana, A.D. Bonev, H.J. Knot, and W.J. Lederer. 1995. Relaxation of arterial smooth muscle by calcium sparks. *Science.* 270:633–637.

Ohi, Y., H. Yamamura, N. Nagano, S. Ohya, K. Muraki, M. Watanabe, and Y. Imaizumi. 2001. Local Ca^{2+} transients and distribution of BK channels and ryanodine receptors in smooth muscle cells of guinea-pig vas deferens and urinary bladder. *J. Physiol.* 534:313–326.

Perez, G.J., A.D. Bonev, J.B. Patlak, and M.T. Nelson. 1999. Functional coupling of ryanodine receptors to K_{Ca} channels in smooth muscle cells from rat cerebral arteries. *J. Gen. Physiol.* 113:229–237.

Perez, G.J., A.D. Bonev, and M.T. Nelson. 2001. Micromolar Ca^{2+} from sparks activates Ca^{2+}-sensitive K^+ channels in rat cerebral artery smooth muscle. *Am. J. Physiol.* 281:C1769–C1775.

Pluger, S., J. Faulhaber, M. Furstenau, M. Lohn, R. Waldschutz, M. Gollasch, H. Haller, F.C. Luft, H. Ehmke, and O. Pongs. 2000. Mice with disrupted BK channel β1 subunit gene feature abnormal Ca^{2+} sparks/STOC coupling and elevated blood pressure. *Circ. Res.* 87:e53–e60.

Singer, J.J., and J.V. Walsh, Jr. 1987. Characterization of calcium-activated potassium channels in single smooth muscle cells using the patch-clamp technique. *Pflugers Arch.* 408:98–111.

Downloaded from www.jgp.org on July 15, 2008

Published June 10, 2002

Somlyo, A.V., and C. Franzini-Armstrong. 1985. New views of smooth muscle structure using freezing, deep-etching and rotary shadowing. *Experientia.* 41:841–856.

Stern, M.D. 1992. Buffering of calcium in the vicinity of a channel pore. *Cell Calcium.* 13:183–192.

Tanaka, Y., P. Meera, M. Song, H.-G. Knaus, and L. Toro. 1997. Molecular constitutes of maxi K_{Ca} channels in human coronary smooth muscle: predominant α + β subunit complexes. *J. Physiol.* 502:545–557.

Wallner, M., P. Meera, and L. Toro. 1999. Molecular basis of fast inactivation in voltage and Ca^{2+}-activated K^+ channels: A transmembrane β-subunit homolog. *Proc. Natl. Acad. Sci. USA.* 96: 4137–4142.

Xiong, Z.L., K. Kitamura, and H. Kuriyama. 1992. Evidence for contribution of Ca^{2+} storage sites on unitary K^+ channel currents in inside-out membrane of rabbit portal vein. *Pflugers Arch.* 420: 112–114.

ZhuGe, R., S.M. Sims, R.A. Tuft, K.E. Fogarty, and J.V. Walsh, Jr. 1998a. Ca^{2+} sparks activate K^+ and Cl^- channels, resulting in spontaneous transient currents in guinea pig tracheal myocytes. *J. Physiol.* 513:711–718.

ZhuGe, R., R.A. Tuft, K.E. Fogarty, and J.V. Walsh, Jr. 1998b. Coupling of voltage-activated Ca^{2+} channels with Ca^{2+} sparks and Ca^{2+} transients in smooth muscle. *J. Gen. Physiol.* 112:113.

ZhuGe, R., R.A. Tuft, K.E. Fogarty, K. Bellve, F.S. Fay, and J.V. Walsh, Jr. 1999. The influence of sarcoplasmic reticulum Ca^{2+} concentration on Ca^{2+} sparks and spontaneous transient outward currents in single smooth muscle cells. *J. Gen. Physiol.* 113: 215–228.

ZhuGe, R., K.E. Fogarty, R.A. Tuft, L.M. Lifshitz, K. Sayar, and J.V. Walsh, Jr. 2000. Dynamics of signaling between Ca^{2+} sparks and Ca^{2+}-activated K^+ channels studied with a novel image-based method for direct intracellular measurement of ryanodine receptor Ca^{2+} current. *J. Gen. Physiol.* 116:845–864.

Downloaded from www.jgp.org on July 15, 2008